Imber Suzanne, Mary (Orcid ID: 0000-0001-7917-8087)
Slavin James, A. (Orcid ID: 0000-0002-9206-724X)

MESSENGER Observations of Magnetotail Loading and Unloading: Implications for Substorms at Mercury

S. M Imber[1,2] and J. A. Slavin[2]

[1] Department of Physics and Astronomy, University of Leicester, Leicester, UK

[2] Department of Atmospheric, Oceanic and Space Sciences, University of Michigan, Ann Arbor, Michigan, USA.

This is the author manuscript accepted for publication and has undergone full peer review but has not been through the copyediting, typesetting, pagination and proofreading process, which may lead to differences between this version and the Version of Record. Please cite this article as doi: 10.1002/2017JA024332

Abstract

We present the first statistical study of loading and unloading of magnetic flux in Mercury's magnetotail. These events describe the global circulation of magnetic flux through the magnetosphere, and provide strong evidence that terrestrial-type substorms take place at Mercury. 438 events were identified over the four years of the MESSENGER mission by a gradual, short-lived increase in the magnetotail lobe magnetic field strength, coincident with an outward flaring of the magnetotail. Substorm duration ranged from tens of seconds to several minutes, with a median of 195 seconds and a mean of 212 seconds. The median amplitude of lobe magnetic field increase was ~11.5 nT, which represents an increase of 23.4% on the background lobe field strength, compared with ~10% for terrestrial substorms. The magnetotail lobes were found to contain ~2-3 MWb of magnetic flux based on 1031 tail passes, with a mean of 2.52 MWb and a standard deviation of 0.48 MWb. An estimate of the change in open flux content during the loading phase of each substorm ranged from 0.08 to 3.7 MWb with a mean value of 0.69 MWb and a standard deviation of 0.38 MWb. These changes in open flux content are an underestimate as the change in magnetotail radius during the events was not accounted for. The maximum lobe flux content during each substorm (~3 MWb) represented ~40% of the total available magnetic flux in the system (~7.5 MWb). During terrestrial substorms, the maximum lobe magnetic flux content is ~10-12% of the total flux from the dipole. A typical substorm at Mercury therefore cycles through a significantly larger fraction of the available magnetic flux than all but the largest substorms at the Earth.

Introduction

The extreme solar wind in the inner heliosphere drives Mercury's highly dynamic magnetosphere. Reconnection between the interplanetary magnetic field (IMF) and the

planetary field enables transfer of energy and momentum to the planetary magnetosphere, allowing solar wind plasma direct entry into the system. Observations of reconnection-related signatures at Mercury's dayside magnetopause were first reported by Russell and Walker (1985) using data from the Mariner 10 mission, which completed three fly-bys of Mercury in the 1970s. Confirmation of these signatures was subsequently made by the MESSENGER spacecraft, which orbited Mercury from 2011 to 2015. The reconnection rate observed during MESSENGER's second planetary flyby was observed to be ~10 times higher than that typically observed at the Earth [Slavin et al, 2009]. DiBraccio et al. (2013) analysed MESSENGER encounters with Mercury's dayside magnetopause, and calculated the ratio of the magnetic field component normal to the surface, to that in the magnetopause plane, to estimate a dimensionless reconnection rate at a single point. This reconnection rate was found to be ~3 times that observed at the Earth, was lower for increasing magnetosheath plasma beta, and independent of the IMF clock angle. Analysis of the magnetosheath plasma properties by Gershman et al. [2013] confirmed the formation of thick plasma depletion layers in the magnetosheath, producing low plasma beta conditions. Observations of Flux Transfer Events (FTEs), helical bundles of reconnected field lines formed at one or multiple magnetopause reconnection sites, have been used to provide a lower limit on the dayside reconnection rate, as well as estimate the rate of magnetic flux transport into the magnetotail during strong dayside driving conditions (Imber et al., 2014). Slavin et al. (2012a) coined the phrase 'FTE showers' to describe a phenomenon unique to Mercury; observations of chains of hundreds of FTEs travelling along the dayside magnetopause, generated by extreme reconnection events, likely at multiple sites on the magnetopause. The occurrence frequency of these FTE showers is thought to be low, however such observations demonstrate the extreme nature of reconnection at Mercury's magnetosphere on the spectrum of solar system dynamics.

The extremely high dayside reconnection rate combined with the small spatial scale of Mercury's magnetosphere allows rapid addition of open magnetic field lines to the magnetotail. These open field lines map to the region surrounding the magnetic poles of the planet, known as the polar cap, which expands and contracts according to the open flux

content of the system (Siscoe and Huang, 1985; Cowley and Lockwood, 1992). Measurements of the spatial extent of the northern cusp have primarily been made using observations of precipitating ion signatures from MESSENGER's Fast Imaging Plasma Spectrometer (FIPS) instrument (Andrews et al., 2007). Zurbuchen et al. (2011) used FIPS data to estimate that the extent of the cusp was 65-75° magnetic latitude during three MESSENGER orbits, while Raines et al. (2014) analysed 518 cusp crossings and observed a cusp range of 30-80°. Winslow et al. (2012) analysed the magnetic signature of the cusp during six months of data to determine that the limits of the northern cusp are 55.8-83.6° in planet centred coordinates, which corresponds to ~66-85° in dipole-centred coordinates. Gershman et al. (2015) used observations of solar energetic particles to identify the polar cap boundary and observed that on the dayside the range of observations spanned 50-70°, while on the nightside the polar cap extended to latitudes of 30-60°. The range of dayside values observed by Gershman et al. correspond to extremes in magnetospheric open flux content of factor of two. These observations are further supported by observations of short-lived (~3 s) depressions in the cusp magnetic field strength, termed cusp plasma filaments, thought to be related to plasma injection into the cusp. These were first identified by Slavin et al. (2014) and further studied by Poh et al. (2016), who conducted a statistical study and found that their location varied from ~55° to 85° magnetic latitude.

Closure of this open magnetic flux takes place through reconnection between open field lines in the northern and southern tail lobes, which generates newly closed field lines that return to the dayside of the planet. The first indirect observations of tail reconnection using MESSENGER data were reported by Slavin et al. (2009), using data from MESSENGER's second flyby. As MESSENGER approached the magnetotail plasma sheet, helical bundles of reconnected field lines known as flux ropes were observed in the magnetometer data. Observations of a series of compressional signatures associated with the motion of flux ropes in the plasma sheet were also made during this flyby, suggesting a recent episode of reconnection in the magnetotail. A study of both the Mariner 10 data and the MESSENGER fly-bys reported further observations of tail reconnection signatures observed near the peak of tail loading-unloading events, analogous to observations of the terrestrial magnetosphere (Slavin et al., 2012b). Both flux ropes and the signature of their compressional effect on the

lobes have been extensively studied at the Earth and shown to be related to tail reconnection [e.g. Slavin et al., 2003; Imber et al., 2011].

Statistical studies of flux ropes in Mercury's plasma sheet have confirmed that such structures are frequently observed in Mercury's magnetotail and play a significant role in the circulation of magnetic flux through the system [DiBraccio et al., 2015; Sun et al., 2016]. Sundberg et al. [2012] reported observations of dipolarisation fronts in Mercury's magnetotail, observing ten events in a four-minute interval. Dipolarisation events are the signature associated with stretched magnetotail field lines returning to a more dipolar configuration following either near-tail current disruption, or reconnection. The frequency of these dipolarisation events is suggestive of periodic episodes of reconnection unloading magnetic flux from Mercury's magnetotail. Sun et al. (2016) also reported observations of dipolarisation fronts associated with loading/unloading events in the magnetotail. Signatures of high energy electron bursts were identified in Gamma-Ray and Neutron Spectrometer (GRNS) data by Baker et al. (2016). These signatures were predominantly identified in the dawn sector of the inner magnetosphere and are thought to be electrons accelerated by reconnection in the near-magnetotail.

MESSENGER observations of the magnetic field strength in the magnetotail during the three MESSENGER flybys contained large amplitude, short duration increases in the lobe field strength, which were interpreted by Slavin et al. (2010b), as analogous to the terrestrial substorm (e.g. Dungey, 1961; Akasofu, 1964; Baker et al., 1996). During substorms, open magnetic flux builds up and is stored in the magnetotail lobes until released by tail reconnection. The rate of change of polar cap area (and therefore tail lobe field strength) depends on the relative rate of dayside and tail reconnection, such that flux only builds up when dayside reconnection dominates, and is only removed when tail reconnection dominates (e.g. Milan et al. 2003). The four intervals identified by Slavin et al. [2010b], had durations of 1-2 minutes, and the lobe field strength increased during the events by a factor of 2-3.5, suggesting that 30-100% of the total magnetic flux available at Mercury was loaded into the magnetotail during those substorms. In this study, we will build on the observations of Slavin et al. (2010b) by analyzing the properties of a large number of substorms observed during the entire four year MESSENGER mission.

Observations

MESSENGER was a NASA mission launched in 2004 and inserted into a highly elliptical, polar orbit about Mercury on 18th March 2011. The primary mission lasted twelve months, during which time the orbital period was fixed at 12 hours. In April 2012, the orbit was adjusted such that the period was shortened to eight hours (Figure 1). In this study we will be using MESSENGER magnetometer data (Anderson et al., 2007) over the time period March 2011-March 2015. With the exception of closest approach during the first two orbits with periapsis on the dayside (hot season orbits), the magnetometer instrument operated at between 1 and 20 Hz throughout the mission.

A typical orbit of MESSENGER is presented in Figure 2 in solar-wind-aberrated Mercury solar magnetospheric (MSM') coordinates. This coordinate system is centered on Mercury's internal dipole field, which is aligned with the spin axis and offset 0.2 R_M (where R_M is Mercury's radius, or 2440 km) to the north of the planet's geographic equator [Anderson et al., 2011, 2012]. The Z' axis points towards magnetic north, X' is opposite to the direction of the mean solar wind velocity in Mercury's frame, and Y' completes the orthogonal set. The orbital velocity of Mercury around the Sun varies from ~38.9 km s^{-1} to 59.0 km s^{-1} due to the ellipticity of the orbit such that the aberration angle is determined for each orbit independently. The radial solar wind velocity was not measured by MESSENGER, so was assumed to be 400 km s^{-1} when calculating the aberration angle. Panels 2a and b are the location of MESSENGER during the specified orbit, in MSM' X-Z and Y-Z coordinates, with the near-Mercury portion of the orbit highlighted in red, and a typical magnetopause and bowshock overlaid for reference (Winslow et al., 2013). The magnetic field measured by the MAG instrument during the red portion of the orbit is presented in panels c-f, in Mercury solar magnetospheric (MSM') coordinates. Several key features are highlighted; the inbound magnetopause crossing, the southern tail lobe, the plasma sheet in the centre of the magnetotail and the spacecraft closest approach to the planet. Flux ropes in the magnetotail and flux transfer events on the magnetopause observed during both inbound and outbound magnetopause crossings are also highlighted. The green shaded region

corresponds to data taken as MESSENGER traversed a portion of the southern lobe of the magnetotail. It can be seen that the lobe field strength was ~40 nT during this interval, and the entry into the plasma sheet at ~08:15 UT may be recognised by both the increase in the variability and the decrease in magnitude of the magnetic field, both of which are due to the presence of a trapped population of plasma on closed field lines.

All tail lobe observations included in this study were made in the southern lobe, as MESSENGER samples similar down-tail distances throughout the mission in this region (~1.5-4 R_M) as shown in Figure 1. Furthermore, these distances correspond to locations of sunward and anti-sunward flux rope observations (Slavin et al., 2009, 2012b; DiBraccio et al., 2015).

Substorm Statistics

Orbits spanning the period March 2011 until March 2015 were analysed in this study, such that 12 months of 12 hour orbits were included and a further 36 months of 8 hour orbits were included. MESSENGER's highly elliptical orbit means that the spacecraft traversed the southern tail lobe primarily in the MSM' Z-direction, and spent up to 75 minutes per orbit making measurements of the tail lobe. To ensure that sufficient time was spent in the lobe to observe events, and to remove passes where the spacecraft grazed the magnetopause during the lobe encounter, only orbits where the entire lobe traversal took place within $-1.25 \leq$ MSM' Y ≤ 1.25 R_M were included. These remaining 1031 magnetotail passes were analysed by eye.

The ground state of Mercury's magnetosphere is depicted schematically in Figure 3a. Loading of the magnetotail with open magnetic flux generates an inflated magnetotail in which the magnetic pressure in the lobes is higher than in the ground state (Figure 3b). The subsequent release of the stored energy in the magnetotail by reconnection between opposing tail lobe field lines returns the system to the ground state and reduces the magnetic field strength in the lobes (Figure 3a). This is analogous to the terrestrial substorm, although is a highly simplified picture, as there are many unanswered questions concerning the timing of substorm-related features, and the combination of variables

controlling the onset (and termination) of near-tail reconnection at the Earth. For simplicity and in line with previous work, we will describe the loading and unloading of magnetic flux into Mercury's magnetotail as a substorm, and identify such events by a transient increase in the total magnetic field strength in the tail lobes combined with a transient outward flaring of the magnetotail.

The set of criteria used to define the events selected for this study are as follows. The minimum duration of the magnetic field enhancement for each event was selected to be 30 seconds, to exclude the passage of flux ropes formed at reconnection sites in the magnetotail, and FTEs on the magnetopause compressing the lobes. Both of these structures generate similar signatures to a loading-unloading event, and have a characteristic duration of a few seconds at Mercury (Slavin et al., 2010b; Slavin et al., 2012a; Imber et al., 2014) so will be excluded by this criterion. Similarly, compression of the magnetopause by a solar wind pressure pulse will generate a compression of the tail lobes, as depicted in Figure 3c. Solar wind pressure pulses may be observed on timescales similar to our substorm events, therefore in order to exclude such events, we consider the elevation angle of the field lines:

$$\tan\theta = \frac{\sqrt{B_Y^2 + B_Z^2}}{B_X} \qquad \text{(Eqn 1)}$$

where the magnetic field is measured in MSM' coordinates. During a substorm the magnetic field lines will start in the ground state (Figure 3a) and will flare outwards due to the increase in the open flux content of the system (Figure 3b) before relaxing back to the ground state again (Figure 3a). During a solar wind pressure pulse (Figure 3c), the field lines will be compressed towards the central plane of the tail, and then released, so the elevation angle signatures for the substorm and the solar wind compression events are opposite to each other. Field lines near the centre of the magnetotail may experience a lower change in elevation angle than those nearer the magnetopause, so the magnitude of the signature will depend on the location of the observing spacecraft. For this substorm study, we required a minimum elevation angle increase of 5^{o}, coincident with an increase in magnetic field strength during the event. This criterion will also remove substorms observed when

MESSENGER was near the plasma sheet, where the elevation angle of the field lines is negative.

The final criterion that was satisfied for a substorm to be identified in this study was that the maximum magnetic field measured during the event had to be more than 10% of the background magnetic field strength in the lobes. This lower boundary removed small amplitude events caused by wave activity or small variations in solar wind velocity.

An example of a series of loading-unloading events that satisfy all of the criteria listed above is shown in Figure 4, which has the same format as Figure 2, with an additional panel displaying the elevation angle of the magnetic field, according to Equation 1. We observe that the flaring angle is much more variable than the individual components of the magnetic field strength, hence a 20 point sliding window is applied to smooth the data. Between 07:23 and 08:03 UTC on 24 August 2011, MESSENGER was near local midnight in the southern lobe of the tail. The magnetic field measured during this time period is displayed in MSM coordinates. Three loading–unloading events are shaded in green, during which the B_z component decreased as the field magnitude rose (loading) followed by an increase in B_z as the magnitude fell (unloading). The elevation of the magnetic field to the equatorial plane shows that the amplitude of the flaring variation for these events was ~10 to 20°. In this manner the magnetic field flared further away from the central axis of the tail when loaded with additional flux, returning to the ground state when unloaded. The duration of the three events are ~385 s, 180 s and 150 s respectively.

The background lobe field, B_{lobe}, is taken as a one minute average of quiet lobe field strength before and after each event, and the relative amplitude of each event is given by:

$$A = 100 * \frac{B_{max} - B_{lobe}}{B_{lobe}} \qquad \text{(Eqn 2)}$$

where B_{max} is the maximum magnetic field measured during the event. This gives a percentage change in the lobe field strength, which can then be used to estimate the change in the total flux content of the tail according to the method used by Slavin et al., (2010b). The change in intensity during the three events highlighted in Figure 4 is 12, 8 and 14 nT respectively, giving amplitudes of 38, 20 and 33%.

Results and Discussion

MESSENGER completed over 4000 orbits of Mercury during its four year mission. These comprised 1031 orbits during which the magnetometer was making measurements, the trajectory of the spacecraft remained within 1.25 R_M of the MSM' Y axis during the southern tail lobe encounters, and the spacecraft encounter with the southern tail magnetopause was identifiable. These crossings were analysed by eye and substorms were identified as a short-lived (>30 s) increase in the total magnetic field strength to a maximum value greater than 1.1 times the background lobe field, coincident with an outward flaring of the field lines of at least 5°. 438 substorms were identified, taking place during 277 orbits. The remaining orbits either contained too much fluctuation in the magnetic field strength or flaring angle to accurately identify a substorm, or were quiet passes. Passes where the magnetopause could not be accurately determined were excluded, as the change in magnetic flux during the substorm could not be accurately determined.

A superposed epoch analysis of the magnetic field signatures of the 438 substorms is presented in Figure 5. Each substorm signature was resampled at 1000 equal time intervals such that the substorm durations were normalised, and the superposed epoch of each component of the magnetic field, the total field, and the elevation angle are presented. The standard error on the mean is shown as a grey shaded region. This analysis presents the 'average' features of a substorm at Mercury, with an elevation angle change of 8°, and an increase in the magnetic field strength of ~25% of the field before and after the event. The superposed epoch analysis represents the average picture, and demonstrates that the examples given in Figure 4 are broadly representative of the population of events selected. Further analysis of the distribution of events around these average values is presented below.

Histograms of the amplitude and durations of the 438 substorms are presented in Figure 6, with the median of the distributions shown by the vertical black arrows. From Figure 6a it can be seen that the median duration of the substorms in this study is 3.25 minutes, or 195 seconds, with a mean of 212 seconds. These durations are of the order of the duration of the three substorms presented in Slavin et al. (2010b), however this larger statistical study includes several events that are significantly longer than this median value.

The duration of an event does not appear to be significantly correlated to the amplitude of the event or the baseline lobe magnetic field strength, perhaps suggesting that it is instead governed by the dayside reconnection rate, which may continue to open magnetic flux even after the onset of tail reconnection. Substorms at the Earth have a typical duration of ~2-3 hours (e.g. Tanskanen, 2009; Mursula et al., 2011; Forsyth et al., 2015 and references therein); 50-100 times longer than those observed at Mercury. The shorter duration of substorms at Mercury is due to a combination of the solar wind characteristics at Mercury's location in the inner heliosphere (leading to an extremely high dayside reconnection rate relative to the Earth), combined with the small spatial scale of the magnetosphere.

The minimum amplitude of a substorm was set to 10% of the background field strength to aid with, and ensure accuracy of, event identification. The median amplitude of the substorm population is 11.5 nT and the smallest event had an increase of 3.7 nT, as a result of the selection criteria described above. The relative amplitude of each substorm was calculated as the deviation from the background lobe field, divided by that lobe field strength (Equation 2), and these relative amplitudes are presented in Figure 6b. The median value for the 428 substorms was 23.4% of the background field strength and the mean was 27.8%. These values are significantly lower than the amplitude of the four loading/unloading events observed by Slavin et al. (2010b), however the larger substorms presented in this study are comparable. These previously published events were all observed on a single pass, therefore may not represent the full range of substorm amplitudes at Mercury. A comparable statistical study of substorms at Earth by Hsu and McPherron (2000) observed an average increase in the total lobe magnetic field strength of 2-3 nT on a baseline of ~25 nT, representing a fractional increase of ~10%. The largest storm-related substorms in the Hsu and McPherron study had a fractional increase in the tail lobe field of 17%. The substorms identified in this paper have an average fractional increase in lobe field strength of 23.4%, with the most extreme examples nearing 100%.

The location of the magnetopause was recorded as MESSENGER entered/exited the southern tail lobe for each of the 1031 tail lobe passes analysed during this study in accordance with the criteria from Winslow et al. (2013). The distribution of measurements of the magnetotail radius are presented in Figure 7a. The cross sectional area of one

hemisphere of the magnetotail was calculated using the magnetotail radius as measured by MESSENGER, and the cross sectional area of the plasma sheet was then subtracted to give the cross sectional area of the magnetotail lobe. The plasma sheet area was estimated to be 0.1 R_M, the average half-thickness of the plasma sheet (Johnson et al., 2012) multiplied by the diameter of the magnetotail (Equation 3). The magnetic field strength measured just inside the magnetopause (B_T) was then combined with this magnetotail lobe cross sectional area to obtain the open flux content of the tail lobes according to the expression:

$$\phi = B_T(\frac{1}{2}\pi R_T^2 - 0.2R_T) \qquad \text{(Eqn 3)}$$

Histograms of open flux content of the tail lobes and the tail radius for all 1031 passes are displayed in Figure 7, demonstrating that the open flux content of the magnetotail is highly variable, with extreme values between ~1 and 4 MWb. The mean value of the tail lobe flux content was 2.50 MWb. This value is slightly lower than that calculated by Johnson et al. (2012), who derived an mean tail flux content of 2.6 MWb using data from 68 of MESSENGER's orbits. 2.5 MWb of open flux corresponds to a polar cap boundary at 60° magnetic latitude, which falls within the range of measurements of the spatial extent of the cusp described earlier.

The total magnetic flux generated by Mercury's dipole that closes outside the planetary surface may be estimated by integrating the dipole magnetic field normal to the planetary surface, over the portion of the planetary surface corresponding to one magnetic hemisphere. The offset of the dipole to the north of the planetary centre by 0.2 R_M must be taken into account. Equivalently, this flux content may be calculated by integrating the magnetic field perpendicular to the magnetic equatorial plane from the planetary surface to infinity. Assuming a dipole moment of 190 nT R_M^3 (Anderson et al., 2012), the total planetary magnetic flux closing outside the planetary surface is ~7.5 MWb. The average magnetic flux in the southern tail lobe during the 1031 magnetotail crossings (2.5 MWb) therefore corresponds to ~33% of the total magnetic flux available in Mercury's magnetosphere.

The amount of open flux just prior to the loading phase of each substorm was calculated using equation 3. The value of magnetic field was taken to be the background lobe field strength recorded just prior to the substorm, and the value of the radius of the tail was taken as that measured when the spacecraft encountered the magnetopause prior to

entry into the tail lobes. These pre-substorm tail flux values are presented in Figure 8a; the mean and median values (2.39 and 2.23 MWb respectively) are slightly lower than the average lobe flux displayed in Figure 7b. MESSENGER may take over an hour to traverse the southern tail lobe, therefore one source of error in the calculation of the lobe magnetic flux content is the assumption that the magnetotail lobe volume is unchanged from the magnetopause encounter, to the start of the substorm. Figure 7a presents an occurrence histogram of the observed radius of the southern magnetotail lobe (assuming a plasma sheet thickness of 0.1 R_M). The observations show that the tail radius may vary by a factor of two (from ~1.5-3 R_M) although the standard deviation of the distribution is only 0.27 R_M. There are two primary reasons why the magnetotail radius could change on these timescales, one is a change in the open flux content of the magnetotail (which, if satisfying the requirements listed above, would be identified as a substorm) and the other is an increase or a decrease in the solar wind ram pressure at Mercury's orbit. Due to the lack of a solar wind monitor at Mercury, changes in the latter cannot be directly observed. The variability of the solar wind magnetic field was analysed by Korth et al. (2011), who focused on the stability of the magnetic field direction and orientation over time periods of two and four hours. This study demonstrated that the variability of the IMF intensity was 5 nT or less over a third of two-hour passes, suggesting that this aspect of the solar wind is likely to be relatively stable over the timescales of several tens of minutes considered here. A similar study for solar wind pressure, the most significant parameter for this study, has not been published to date.

The amount of open flux added to the system in the loading phase of each substorm is displayed in Figure 8b, assuming that the magnetotail radius does not change significantly during the substorm. The x-axis labels at the top of each panel show the distribution as a percentage of the total magnetic flux available from the dipole (calculated earlier to be 7.5 MWb). The median value of open flux transferred to the magnetotail during a substorm was found to be 0.59 MWb, as indicated by the vertical black arrow, which corresponds to an opening of ~8% of the total available magnetic flux from the dipole. If the net flux increase during the loading phase of a substorm is 0.59 MWb then given the substorm durations presented in Figure 6, the mismatch in the dayside and tail reconnection rates is ~6 kV.

Adding Figure 8a and b together gives an estimate of the open flux content of the lobes just prior to the unloading phase, and these flux values are presented in Figure 8c. At the end of the loading phase of a substorm, the median value of magnetic flux contained within the lobes was found to be 2.95 MWb, with a mean of 3.09 MWb and a standard deviation of 0.94 MWb. Given a total magnetic flux of ~7.5 MWb (calculated above), at the height of an average substorm the magnetotail lobes contain ~40% of the total magnetic flux available from the dipole (see the upper axis of Figure 8c), and in extreme cases can contain a significantly larger fraction than this. This value is significantly higher than the 10-12% observed during the largest terrestrial substorms (e.g. Milan et al., 2004), likely due to the extremely high dayside reconnection rate at Mercury, and the small scale size of the system, allowing closed magnetic flux to be rapidly opened and transported into the magnetotail. If the magnetotail lobes contain on average 2.95 MWb of flux at the peak of a substorm (Figure 8c), then the corresponding latitude of the polar cap would be 55°, representing a change in latitude of 6° from the pre-substorm polar cap latitude (61°). During the largest substorms however, the lobes contain ~80% of the available flux from the dipole, corresponding to a polar cap boundary at ~33° magnetic latitude and a change in polar cap area of a factor of three. This extreme case is in broad agreement with the lowest measured values of the cusp latitude discussed in earlier studies (Raines et al., 2014; Gershman et al., 2015).

The very large range of values of open flux in the magnetotail presented in Figure 8c suggests that there is no threshold open flux content that, when reached, represents an unsustainable limit, and leads to rapid unloading of the system. Rather the unloading phase is observed to begin at a wide range of values of open flux. This is analogous to the current understanding of substorm onset at the Earth, where the auroral brightening corresponding to the onset of tail reconnection may be observed on an expanded, or a contracted auroral oval (e.g. Milan et al., 2008). A complex combination of internal and external system parameters must govern the timing of reconnection onset in the magnetotail at the Earth and at Mercury, and more work is required to understand the interplay between these parameters.

Finally, many passes were observed in which the lobe magnetic field strength did not change appreciably as MESSENGER traversed the lobe. This could be because the dayside reconnection rate was low, although frequently the corresponding encounter with the magnetopause and tail plasma sheet yielded reconnection-related signatures. Another possible explanation for these quiet lobe orbits is that during these times the dayside and the tail reconnection rates were approximately balanced, a state known at the Earth as Steady Magnetospheric Convection (SMC) (e.g. Pytte et al., 1978, DeJong et al., 2008). These lobe crossings will be investigated further in a future manuscript.

Conclusions

438 substorms were identified during four years of MESSENGER encounters with Mercury's southern magnetotail lobe. The median duration of the substorms was found to be 195 seconds, the median relative amplitude was 24% of the background lobe field strength, and during these substorms the change in the open magnetic flux content of the tail lobes was estimated to be in the range 0.2-2 MWb, with a median value of 0.59 MWb, although these calculations are underestimates of the true change in open flux content, as they do not account for the changing tail radius. These substorms are a factor of 50-100 times shorter than those observed at the Earth, however the amplitude of the events in this study (measured as the fractional change in lobe magnetic field strength) was found to be 2-3 times higher than for terrestrial substorms. This comparison demonstrates the combined affect of Mercury's location in the inner solar system (through strong solar wind driving), and the weak instrinsic dipole, which generates a magnetosphere that is much smaller than the magnetosphere of the Earth. These substorms represent a key measure of the global reconnection-driven dynamics in Mercury's magnetosphere, and demonstrate the global implications of the extreme reconnection rates observed in earlier studies of localized reconnection signatures.

Acknowledgements

SMI was supported by The Leverhulme Trust and STFC grant ST/K001000/1. The contributions by JAS were supported by NASA's Heliophysics Supporting Research (NNX15AJ68G) and Living With a Star (NNX16AJ67G) programs. The MESSENGER data used in this paper are available from NASA's Planetary Data System.

Figure Captions

Figure 1. MESSENGER's trajectory during both warm and hot season orbits are plotted in MSM X-Z coordinates. The hot season orbits have closest approach on the dayside of the planet, and the 12-hour orbits are shown in blue, with the 8-hour orbits in green. A model magnetopause and bowshock from Winslow et al. (2013) are plotted for reference.

Figure 2. A typical orbit of MESSENGER through Mercury's magnetosphere. The trajectory of MESSENGER during the interval 06:50-09:50 UT on August 24 2011 is highlighted in red in aberrated solar wind coordinates projected into the a) X-Y and b) X-Z planes. c-d) The magnetic field measured by MESSENGER data during the same time interval is presented in MSM coordinates.

Figure 3. A schematic to show a) the ground state of Mercury's magnetosphere b) Mercury's inflated magnetosphere following a period of loading of magnetic flux into the magnetotail, and c) The effect of a solar wind pressure pulse or a tailward-moving flux transfer event on the magnetotail magnetic field lines.

Figure 4. MESSENGER's trajectory and corresponding magnetic field data in the same format as presented in Figure 2. The 40 minutes of data correspond to the highlighted green portion of Figure 2, and three substorms are selected during this interval.

Figure 5. A superposed epoch analysis of the magnetic field signatures of the 438 substorms identified in this study, normalised according to the duration of each event. Panels a) – d) are the magnetic field components in aberrated MSM coordinates and the total field strength. Panel e) is the elevation angle of the tail lobe magnetic field, as defined in Equation 2. The grey shaded regions are the standard error on the mean, given by the standard deviation of the distribution divided by the square root of the number of observations.

Figure 6. Histograms of a) the duration and b) the amplitude of the 438 substorms. The median values of 195 seconds and 23.4% amplitude are highlighted by the vertical black arrows.

Figure 7. Histograms of a) the radius and b) the open flux content of the magnetotail during the 1031 magnetotail passes included in this study. The median values of the distributions are highlighted by the vertical black arrows.

Figure 8. Histograms of a) the open flux content of the magnetotail prior before (and after) the 438 substorms, b) the change in open flux content during the loading phase of the substorms c) the maximum open flux during the substorms. The median values are highlighted by the vertical black arrows. The upper x-axis labels convert the flux values to a percentage of the available magnetic flux leaving the planetary surface (7.5 MWb).

References

Akasofu, S.-I. (1964), The development of the auroral substorm, *Planet. Space Sci.*, 12, 273–282, doi:10.1016/0032-0633(64)90151-5.

Anderson, B. J., M. H. Acuña, D. A. Lohr, J. Scheifele, A. Raval, H. Korth, and J. A. Slavin (2007), The Magnetometer instrument on MESSENGER, *Space Sci. Rev., 131,* 417–450, doi:10.1007/s11214-007-9246-7.

Anderson, B. J., C. L. Johnson, H. Korth, M. E. Purucker, R. M. Winslow, J. A. Slavin, S. C. Solomon, R. L. McNutt Jr., J. M. Raines, and T. H. Zurbuchen (2011), The global magnetic field of Mercury from MESSENGER orbital observations, *Science, 333*, 1859–1862, doi:10.1126/science.1211001.

Anderson, B. J., C. L. Johnson, H. Korth, R. M. Winslow, J. E. Borovsky, M. E. Purucker, J. A. Slavin, S. C. Solomon, M. T. Zuber, R. L. McNutt Jr., (2012), Low-degree structure in

Mercury's planetary magnetic field, *J. Geophys. Res.*, 117, E00L12, doi:10.1029/2012JE004159.

Andrews, G. B., et al. (2007), The energetic particle and plasma spectrometer instrument on the MESSENGER spacecraft, *Space Sci. Rev.*, **131**, 523–556, doi:10.1007/s11214-007-9272-5.

Baker, D. N., T. I. Pulkkinen, V. Angelopoulos, W. Baumjohann, and R. L. McPherron (1996), Neutral line model of substorms: Past results and present view, *J. Geophys. Res.*, 101, 12,975–13,010, doi:10.1029/95JA03753.

Cowley, S. W. H., and Lockwood, M. (1992), Excitation and decay of solar wind-driven flows in the magnetosphere-ionosphere system, *Ann. Geophys., 10*, 103–115.

DeJong, A. D., A. J. Ridley, and C. R. Clauer (2008), Balanced reconnec- tion intervals: Four case studies, *Ann. Geophys.,* 26, 3897–3912, doi:10.5194/angeo-26-3897-2008.

DiBraccio, G. A., J. A. Slavin, S. A. Boardsen, B. J. Anderson, H. Korth, T. H. Zurbuchen, J. M. Raines, D. N. Baker, R. L. McNutt Jr., *and* S. C. Solomon (2013), MESSENGER observations of magnetopause structure and dynamics at Mercury, *J. Geophys. Res. Space Physics, 118, 997–1008, doi:*10.1002/jgra.50123.

DiBraccio, G. A., Slavin, J. A., Imber, S. M., Gershman, D. J., Raines, J. M., Jackman, C. M., ... Solomon, S. C. (2015). MESSENGER observations of flux ropes in Mercury's magnetotail. Planetary and Space Science, 115, 77-89. [3883]. DOI: 10.1016/j.pss.2014.12.016

Dungey, J. W. (1961), Interplanetary magnetic fields and the auroral zones, *Phys. Rev. Lett.*, 6, 47–48, doi:10.1103/PhysRevLett.6.47.

Forsyth, C., I. J. Rae, J. C. Coxon, M. P. Freeman, C. M. Jackman, J. Gjerloev, and A. N. Fazakerley (2015), A new technique for determining Substorm Onsets and Phases from

Indices of the Electrojet (SOPHIE), *J. Geophys. Res. Space Physics*, 120, 10,592–10,606, doi:10.1002/2015JA021343.

Gershman, D. J., J. A. Slavin, J. M. Raines, T. H. Zurbuchen, B. J. Anderson, H. Korth, D. N. Baker, and S. C. Solomon (2013), Magnetic flux pileup and plasma depletion in Mercury's subsolar magnetosheath, *J. Geophys. Res. Space Physics, 118,* 7181–7199, doi:10.1002/2013JA019244.

Gershman, D. J., et al. (2015), MESSENGER observations of solar energetic electrons within Mercury's magnetosphere, *J. Geophys. Res. Space Physics*, 120, 8559–8571, doi:10.1002/2015JA021610.

Hsu, T.-S., and R. L. McPherron, The characteristics of storm-time substorms and non-storm substorms, Proceedings of the International Conference on Substorms (ICS-5), *Eur. Space Agency, Spec. Publ., ESA SP-443*, 439, 2000.

Imber, S. M., J. A. Slavin, S. A. Boardsen, B. J. Anderson, H. Korth, R. L. McNutt Jr., and S. C. Solomon (2014), MESSENGER observations of large dayside flux transfer events: Do they drive Mercury's substorm cycle?, *J. Geophys. Res. Space Physics*, 119, 5613–5623, doi:10.1002/2014JA019884.

Korth, H., B. J. Anderson, T. H. Zurbuchen, J. A. Slavin, S. Perri, S. A. Boardsen, R. L. McNutt Jr. (2011), The interplanetary magnetic field environment at Mercury's orbit. Planetary and Space Science, 59(15), 2075-2085. DOI: 10.1016/j.pss.2010.10.014

Milan, S. E., M. Lester, S. W. H. Cowley, K. Oksavik, M. Brittnacher, R. A. Greenwald, G. Sofko, and J.-P. Villain, Variations in polar cap area during two substorm cycles, *Ann. Geophys.,* 21, 1121-1140, 2003.

Milan, S. E., S. W. H. Cowley, M. Lester, D. M. Wright, J. A. Slavin, M. Fillingim, C. W. Carlson, and H. J. Singer (2004), Response of the magnetotail to changes in the open flux content of the magnetosphere, *J. Geophys. Res.,* 109, A04220, doi:10.1029/2003JA010350.

Mursula, K., E. Tanskanen, and J. J. Love (2011), Spring-fall asymmetry of sub- storm strength, geomagnetic activity and solar wind: Implications for semiannual variation and solar hemispheric asymmetry, *Geophys. Res. Lett.,* 38, L06104, doi:10.1029/2011GL046751.

Poh, G., et al. (2016), MESSENGER observations of cusp plasma filaments at Mercury*, J. Geophys. Res. Space Physics*, 121, 8260–8285, doi:10.1002/2016JA022552.

Pytte T, McPherron RL, Hones EW, West HL Jr (1978) Multiple satellite studies of magnetospheric substorms: distinction between polar magnetic substorms and convection-driven bays. *J Geophys Res.* 83:663

Raines, J. M., D. J. Gershman, J. A. Slavin, T. H. Zurbuchen, H. Korth, B. J. Anderson, G. Gloeckler, and S. C. Solomon (2014), Structure and dynamics of Mercury's magnetospheric cusp: MESSENGER measurements of protons and planetary ions, *J. Geophys. Res. Space Physics*, **119**, 6587–6602, doi:10.1002/2014JA020120.

Russell, C. T.*, and* R. J. Walker (1985)*,* Flux transfer events at Mercury*, J. Geophys. Res., 90,* 11,067–11,074*, doi:*10.1029/JA090iA11p11067*.*

Shue, J.-H., J. K. Chao, H. C. Fu, C. T. Russell, P. Song, K. K. Khurana, and H. J. Singer (1997), A new functional form to study the solar wind control of the magnetopause size and shape, *J. Geophys. Res.*, 102 (1), 9497, doi:10.1029/97JA00196.

Siscoe, G. L., and T. S. Huang (1985), Polar cap inflation and deflation, *J. Geophys. Res.,* 90(A1), 543–547, doi:10.1029/JA090iA01p00543.

Slavin, J. A., R. P. Lepping, J. Gjerloev, D. H. Fairfield, M. Hesse, C. J. Owen, M. B. Moldwin, T. Nagai, A. Ieda, and T. Mukai (2003), Geotail observations of magnetic flux ropes in the plasma sheet*, J. Geophys. Res*., *108*(A1), 1015, doi:10.1029/2002JA009557.

Slavin, J. A., et al. (2009), MESSENGER observations of magnetic reconnection in Mercury's magnetosphere, *Science, 324*, 606–610, doi:10.1126/science.1172011.

Slavin, J. A., et al. (2010b), MESSENGER observations of extreme loading and unloading of Mercury's magnetic tail*, Science, 329,* 665–668.

Slavin, J. A., et al. (2010a), MESSENGER observations of large flux transfer events at Mercury, *Geophys. Res. Lett.*, *37*, L02105, doi:10.1029/2009GL041485.

Slavin, J. A., S. M. Imber, S. A. Boardsen, G. A. DiBraccio, T. Sundberg, M. Sarantos, T. Nieves-Chinchilla, A. Szabo, B. J. Anderson, H. Korth, T. H. Zurbuchen, J. M. Raines, C. L. Johnson, R. M. Winslow, R. M. Killen, R. L. McNutt, Jr., and S. C. Solomon (2012a), MESSENGER Observations of a Flux Transfer Shower at Mercury, *J. Geophys. Res., 117*, A00M06, doi:10.1029/2012JA017926.

Slavin, J. A., B. J. Anderson, D. N. Baker, M. Benna, S. A. Boardsen, R. E. Gold, G. C. Ho, S. M. Imber, H. Korth, S. M. Krimigis, R. L. McNutt, Jr, J. M. Raines, M. Sarantos, D. Schriver, S. C. Solomon, P. Trávníček, and T. H. Zurbuchen (2012b), MESSENGER Flyby Observations of Magnetotail Structure and Dynamics at Mercury, *J. Geophys. Res., 117*, A01215, doi:10.1029/2011JA016900.

Sun, W. J., S. Y. Fu, J. A. Slavin, J. M. Raines, Q. G. Zong, G. K. Poh, and T. H. Zurbuchen (2016), Spatial distribution of Mercury's flux ropes and reconnection fronts: MESSENGER observations, *J. Geophys. Res. Space Physic*s, 121, doi:10.1002/2016JA022787.

Sundberg, T., J. A. Slavin, S. A. Boardsen, B. J. Anderson, H. Korth, G. C. Ho, D. Schriver, V. M. Uritsky, T. H. Zurbuchen, J. M. Raines, D. N. Baker, S. M. Krimigis, R. L. McNutt Jr., and S. C. Solomon (2012), MESSENGER observations of dipolarization events in Mercury's magnetotail, *J. Geophys. Res.*, 117, A00M03, doi:10.1029/2012JA017756.

Tanskanen, E. I. (2009), A comprehensive high-throughput analysis of substorms observed by IMAGE magnetometer network: Years 1993–2003 examined, *J. Geophys. Res.,* 114, A05204, doi:10.1029/2008JA013682.

Winslow, R. M., C. L. Johnson, B. J. Anderson, H. Korth, J. A. Slavin, M. E. Purucker, and S. C. Solomon (2012), Observations of Mercury's northern cusp region with MESSENGER's Magnetometer, *Geophys. Res. Lett.,* 39, L08112, doi:10.1029/2012GL051472.

Winslow, R. M., B. J. Anderson, C. L. Johnson, J. A. Slavin, H. Korth, M. E. Purucker, D. N. Baker, *and* S. C. Solomon (2013), Mercury's magnetopause and bow shock from MESSENGER Magnetometer observations, *J. Geophys. Res. Space Physics, 118, 2213–2227, doi:*10.1002/jgra.50237.

Zurbuchen, T. H., et al. (2011), MESSENGER observations of the spatial distribution of planetary ions near Mercury, *Science*, **333**, 1862–1865, doi:10.1126/science.1211302.

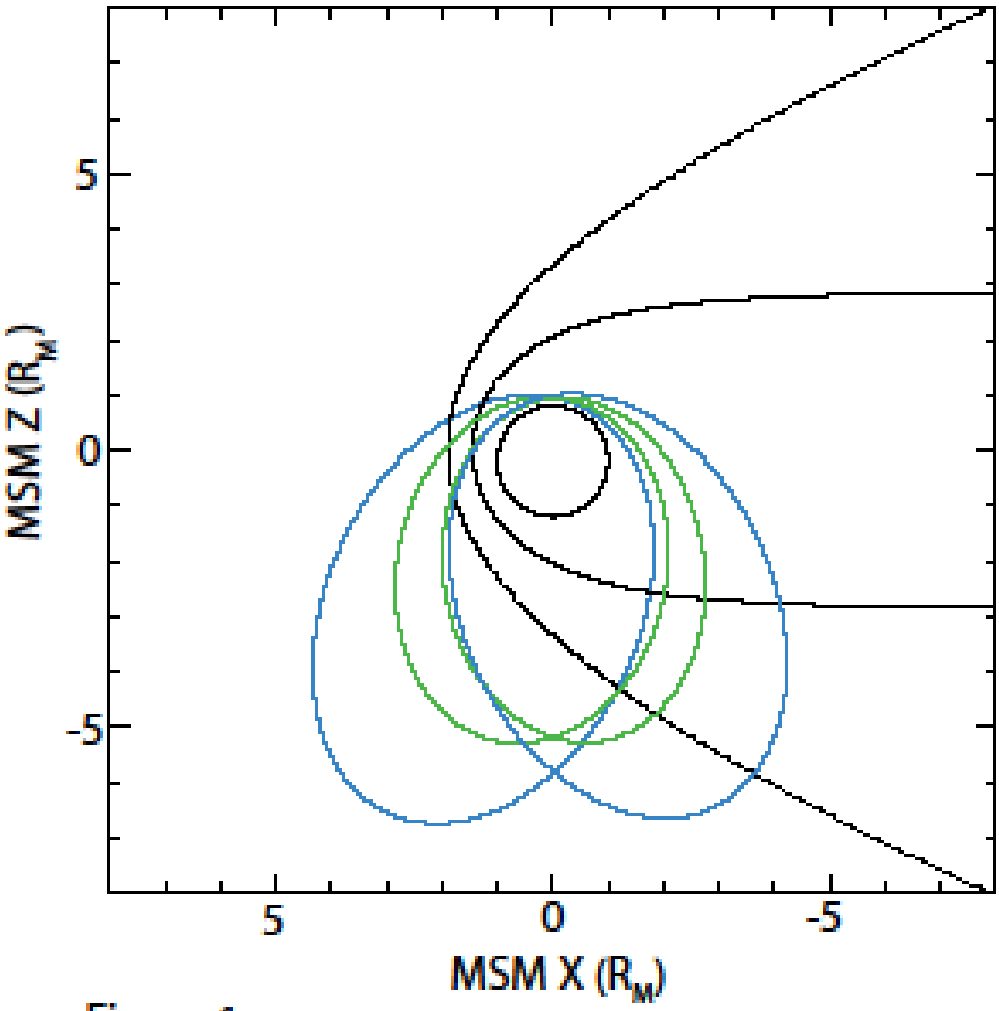

Figure 1

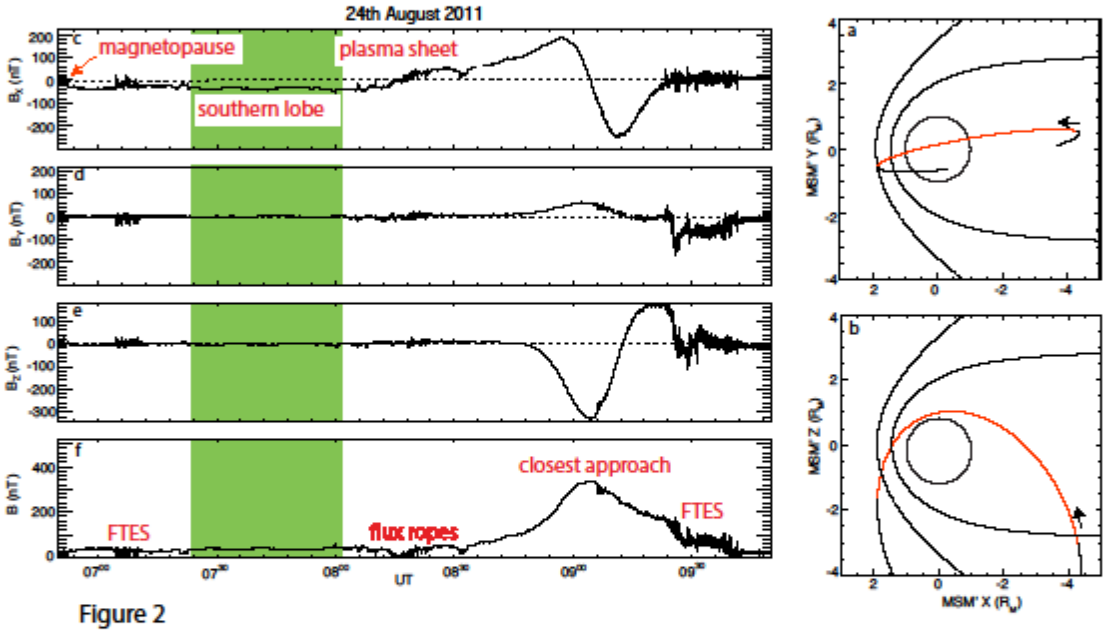

Figure 2

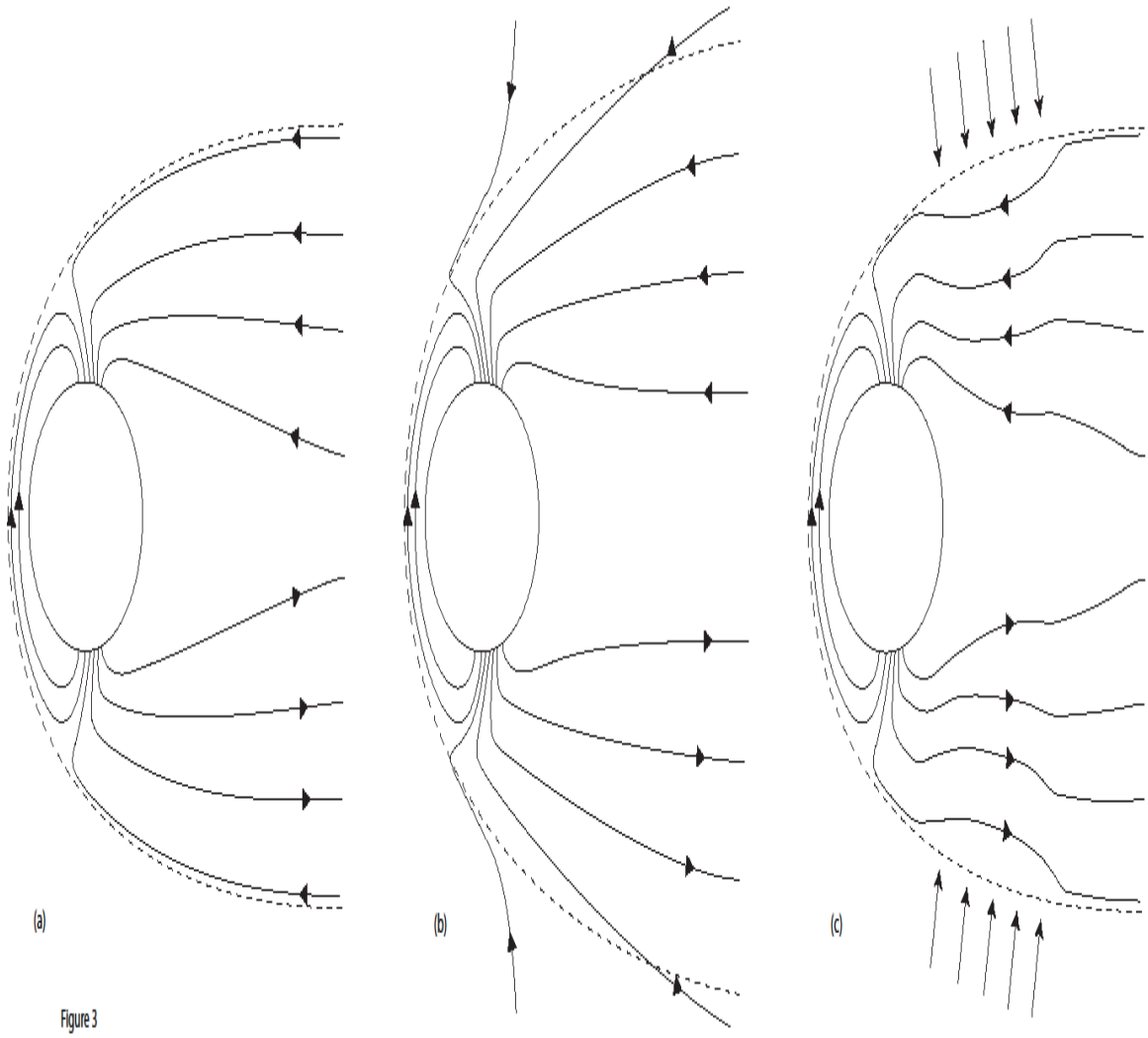

Figure 3

Fig 3

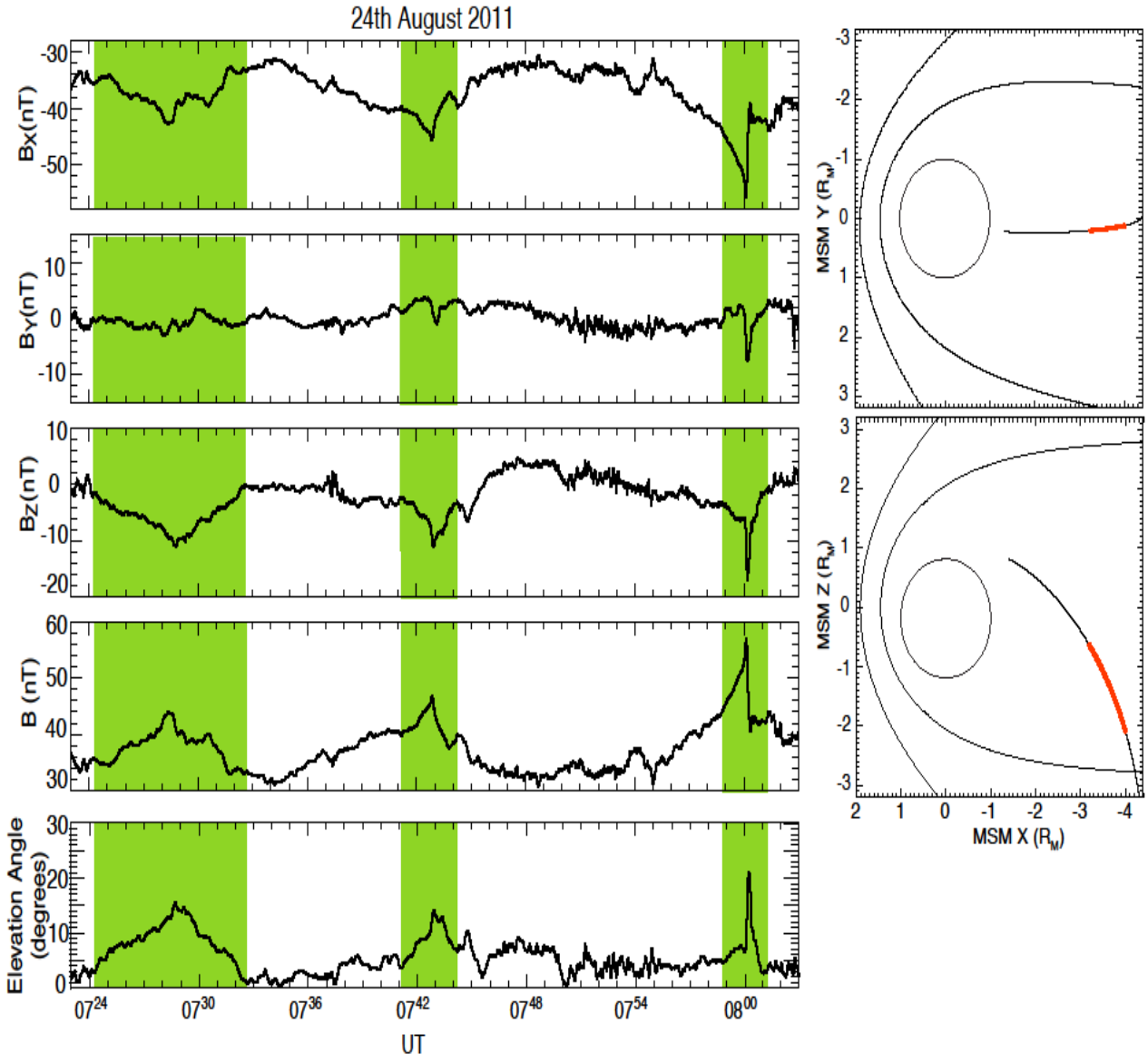

Figure 4

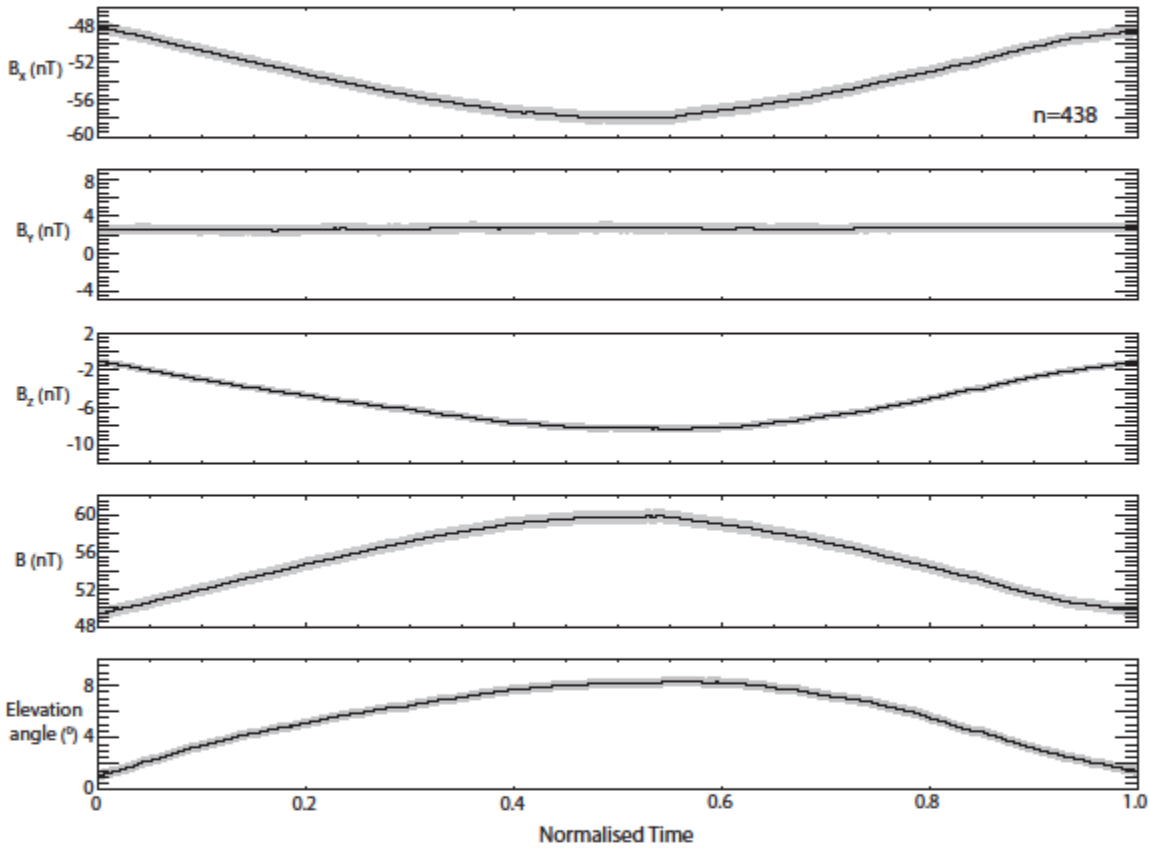

Figure 5

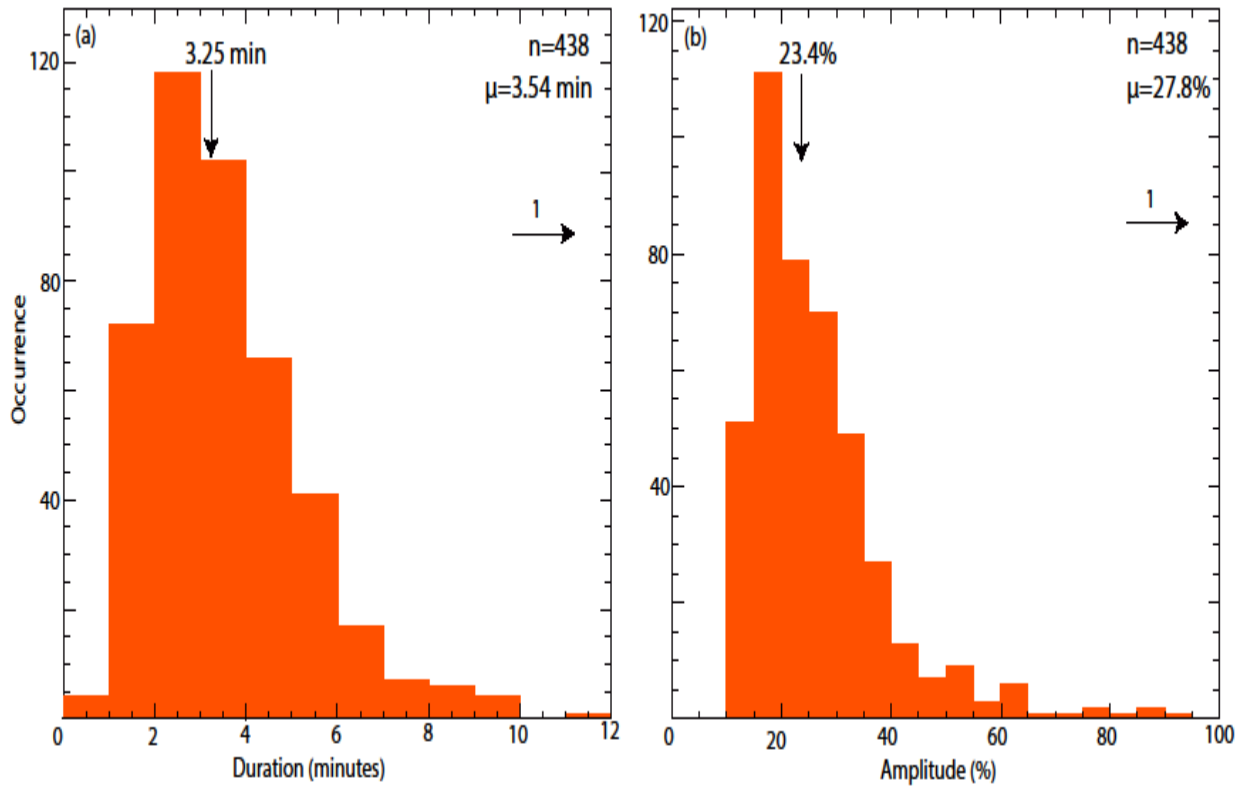

Figure 6

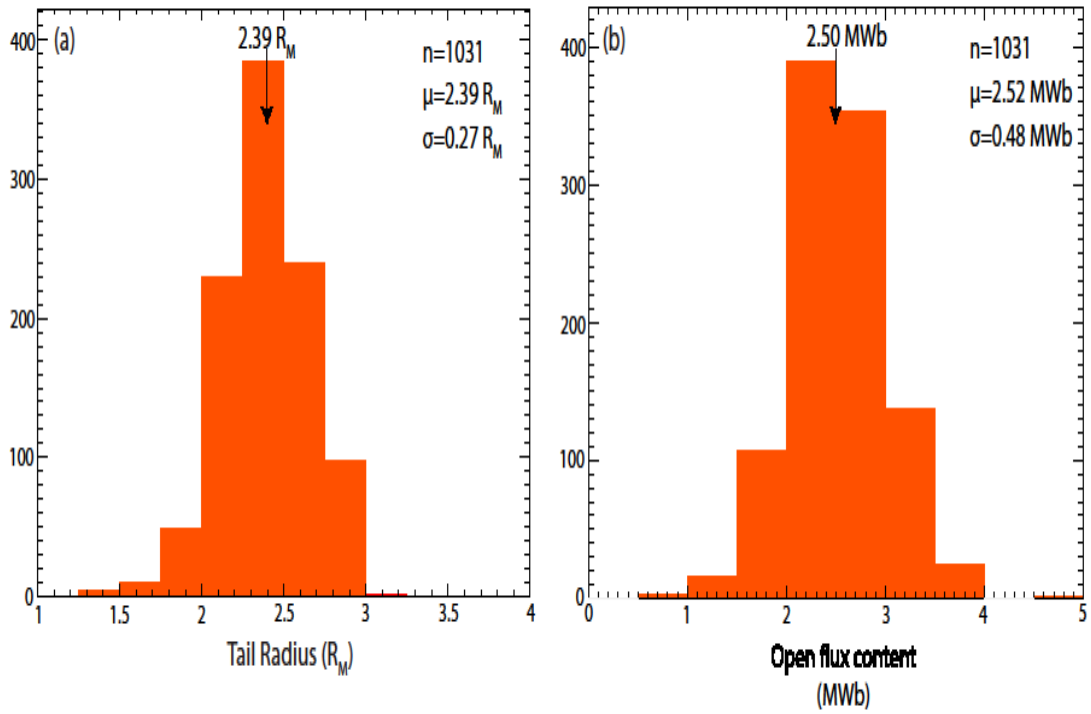

Figure 7

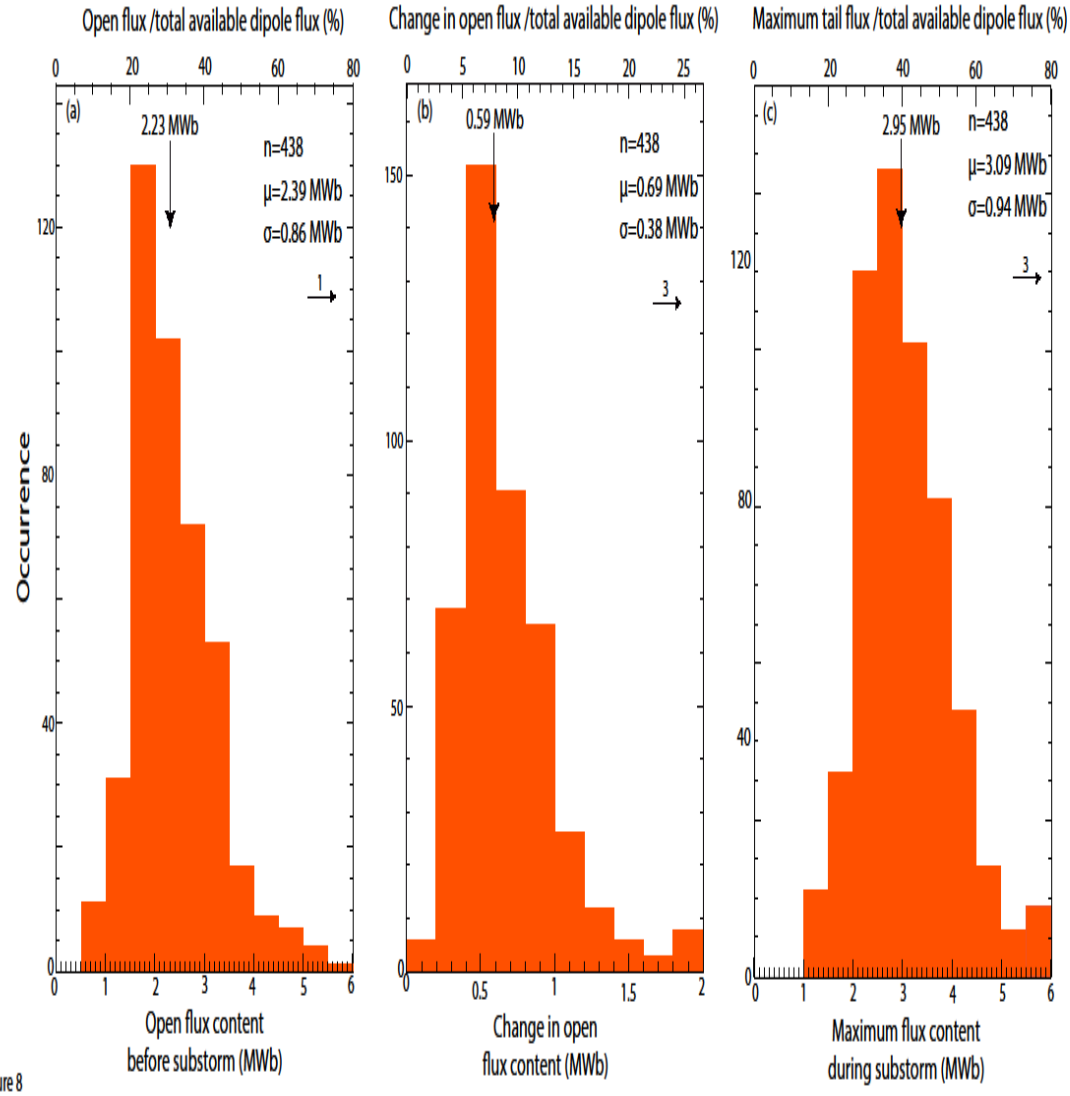

Figure 8